Book Title
Book Editors
IOS Press, 2003

Robot-assisted Needle Placement in Open-MRI: System Architecture, Integration and Validation

S.P. DiMaio [a,1], S. Pieper [b], K. Chinzei [c], N. Hata [a], E. Balogh [d], G. Fichtinger [d], C.M. Tempany [a], R. Kikinis [a],

[a] *Brigham and Women's Hospital, Harvard Medical School*
[b] *Isomics Inc.*
[c] *National Institute of Advanced Industrial Science and Technology, Japan*
[d] *Johns Hopkins University*

Abstract. This work describes an integrated system for planning and performing percutaneous procedures—such as prostate biopsy—with robotic assistance under MRI-guidance. The physician interacts with a planning interface in order to specify the set of desired needle trajectories, based on anatomical structures and lesions observed in the patient's MR images. All image-space coordinates are automatically computed, and used to position a needle guide by means of an MRI-compatible robotic manipulator, thus avoiding the limitations of the traditional fixed needle template. Direct control of real-time imaging aids visualization of the needle as it is manually inserted through the guide. Results from in-scanner phantom experiments are provided.

Keywords. robot-assisted needle biopsy, MR-compatible robot, prostate cancer

1. Introduction

Accurate navigation of surgical instruments (e.g., biopsy and therapy needles), based on pre-operative trajectory plans and intra-operative guidance, is a challenging problem in image-guided therapy. Stereotactic frames and needle template guides are typically used to calibrate and constrain instrument motion, but often lead to inflexible guidance mechanisms and workflows. In this work, we focus on prostate biopsy and brachytherapy procedures that are currently performed under MRI guidance at the Brigham and Women's Hospital [1]. Similarly to the standard transrectal-ultrasound-guided approaches, these procedures rely on a fixed needle template guide that constrains trajectory resolution and orientation.

MRI is an attractive choice for image-guidance, due to its excellent soft tissue contrast, multi-parametric imaging protocols, high spatial resolution, and mul-

[1]Correspondence to: Simon DiMaio, Brigham and Women's Hospital, 75 Francis Street, Boston, 02115. E-mail: simond@bwh.harvard.edu

tiplanar volumetric imaging capabilities. The peripheral zone (PZ) can be seen in T2-weighted images, and used to identify suspicious nodules in the peripheral zone. A multi-year clinical trial of MRI-guided prostate biopsy is described in [2], and uses an intra-operative open 0.5 tesla MR imager (GEMS Signa SP). While the use of MRI imaging in prostate cancer biopsy and therapy appears to have helped improve outcomes, the manual method of needle placement has remained unchanged. The use of a fixed needle guide template, with holes spaced at least 5mm apart, limits needle trajectory position and orientation. In addition, template registration and the manual computation and transcription of coordinates are prone to human error. *This paper introduces a system that integrates an interactive planning system and real-time imaging control interface with an MR-compatible robotic assistant that acts as a dynamic needle guide for precise, yet flexible targeted needle placement. The system has been validated for a prostate biopsy procedure, and approved for a first clinical trial. It is based on an a modular and extensible architecture.*

Robotic assistance has been investigated for guiding instrument placement in MRI, beginning with neurosurgery [3] and later percutaneous interventions [4, 5]. Chinzei et al. developed a general-purpose robotic assistant for open MRI [6] that was subsequently adapted for transperineal intra-prostatic needle placement [7]. Krieger et al. presented a 2-DOF passive, un-encoded and manually manipulated mechanical linkage to aim a needle guide for transrectal prostate biopsy with MRI guidance [8]. With three active tracking coils, the device is visually servoed into position and then the patient was moved out of the scanner for needle insertion. Other recent developments in MRI-compatible mechanisms include haptic interfaces for fMRI [9] and multi-modality actuators and robotics [10].

This paper is organized as follows: Section 2 describes the architecture of the robot-assisted system that includes a planning interface and an MRI-compatible needle positioning device (Section 3). Preliminary results from in-scanner phantom tests are given in Section 4. Concluding remarks are provided in Section 5.

2. System Architecture

The architecture of the MR-guided, robot-assisted percutaneous intervention system is shown in Figure 1. The three major subsystems, namely the planning environment, the MR scanner (GE Signa SP, Milwaukee WI), and the motion controlled robotic manipulator, are integrated as shown. The workflow is as follows:

1. Visualize pre-procedural MR images I_{MRI} to specify a set of biopsy targets. Image visualization and target planning are performed using the 3D Slicer [11]. For each biopsy plan, the physician specifies two points along the needle trajectory, namely a target and an entry point, by clicking on coordinates on T2-weighted images viewed in the Slicer.
2. The robot is visualized in conjunction with the images and the biopsy plan, and positioning motions can be simulated and rendered on-screen for trajectory verification.
3. Calibrate robot to image space using a Flashpoint® optical tracking system.
4. Execute robot joint-space motion commands (q, $\dot{q}$, $\ddot{q}$) via an ethernet connection with the robot controller.
5. Robot motion proceeds and is continuously monitored and compared against a simulated robot motion model; any significant trajectory deviation halts motion.

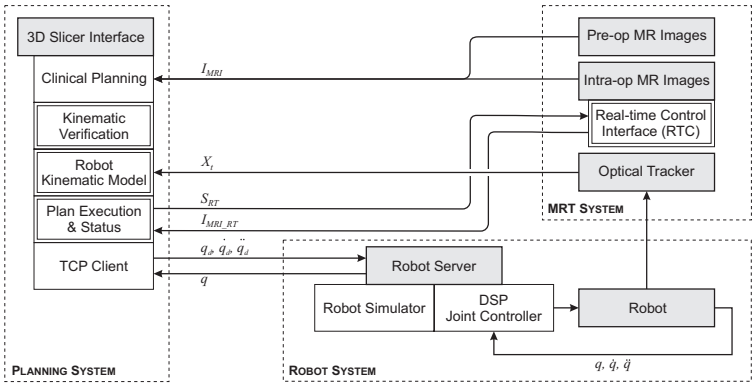

Figure 1. The percutaneous intervention system, comprised of a planning sub-system, the MRT, and an MR-compatible robot.

6. Verify robot position by comparing the optically tracked needle guide position (X_t) with the biopsy plan. Steps 4-6 are repeated until the positioning error is satisfactorily compensated.
7. Imaging plane coordinates (S_{RT}) corresponding to the plane of the needle are sent from the 3D Slicer to the scanner's Real Time Control interface, and real-time images (I_{MRI_RT}) are aquired and displayed.
8. The needle is manually inserted through the needle guide, under real-time MR guidance (3-6s image update), and a biopsy sample is taken. Steps 4-8 are repeated until all target sites have been sampled.

3. MRI-compatible Needle Positioning Device

For this work, we use a first-generation MRI-compatible robotic assistant developed by [12–14] for use in a Magnetic Resonance Therapy operating room (MRT) equipped with a GE SIGNA SP open-MRI scanner. The robotic device consists of five linear motion stages arranged to form a 2-DOF orienting mechanism attached to a 3-DOF Cartesian positioning mechanism. The base of the robot is mounted above the surgeon's head in the open MRI magnet and two rigid arms reach down into the surgical field. The ends of the arms are linked to form a tool holder, which in this case is a linear needle guide (Figure 2(b)). There is a Flashpoint® optical marker attached to the needle guide, providing independent redundant encoding of end-effector pose, as shown in Figure 2(b-inset). The mechanism is constructed almost entirely from non-ferrous, MR-compatible materials. The gantry frame is composed of aluminum and titanium elements, and each linear motion stage comprises plastic, titanium, stainless steel (YHD50) and beryllium-copper (Be-Cu) components. All sensors are optical and signals are transferred to and from the magnet room via fiber-optics. Linear optical encoders measure the displacement of each motion stage with 20μm resolution (Encoder Technology, Cottonwood, AZ). The actuators are ultrasonic motors (Shinsei travelling-wave USR60 USM) that contain no magnetic or ferrous components. The MRI compatibility of the robotic mechanism was evaluated in the open-MR scanner and found to produce no adverse effects. In fact, the robot created less field distortion than the body of the patient, as measured by [13].

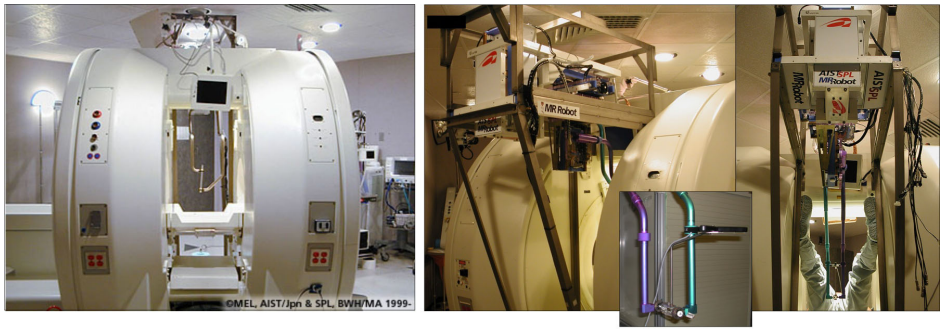

(a) (b)

Figure 2. (a) GE Signa SP open-MRI scanner, with (b) integrated 5-DOF MR-compatible robot. The robot end-effector is equipped with an optical tracking marker (inset).

4. Phantom Experiments

Needle placement has been verified using a polyvinyl chloride (PVC) tissue phantom measuring $9 \times 9 \times 11$cm. The phantom incorporates a prostate model, as well as several acrylic beads that serve as targets. The beads have a hole diameter of 3mm, and are embedded at depths up to 9cm from the inferior surface of the phantom. The tissue phantom was placed into a patient leg model, as shown in Figure 3(a), and transferred into the MRI scanner in order to mimick the clinical procedure. Sterile draping is applied to both the patient model and the robot manipulator arms, as shown in Figure 3(b). The phantom was scanned and the image volume imported into the 3D Slicer for planning and placement, as described in Section 2, and shown in Figure 3(c). In this study, we attempted to

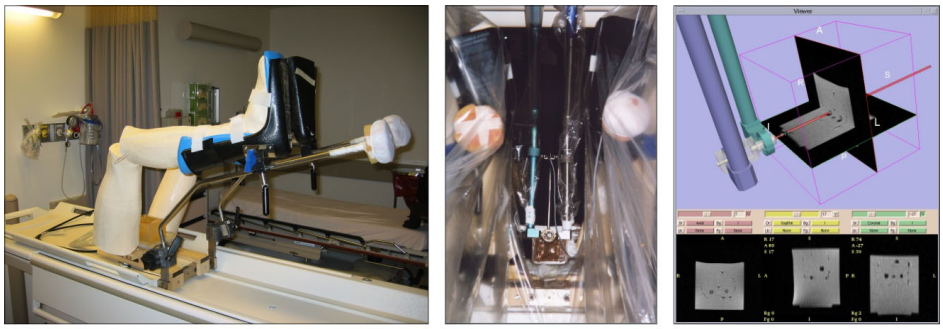

(a) (b) (c)

Figure 3. Phantom experiments: (a) scale models of legs and PVC prostate phantom with embedded targets, (b) patient model and robot placement inside the scanner, with sterile draping, (c)needle trajectories are interactively specified in the planning environment.

place 10 needles (E-Z-EM Inc., MRI Histology) into the centres of the beads from a variety of different trajectory angles. 7 needles were placed into centres of the beads, while 2 needles hit the sides of their target beads. One needle, which was targeted along an elevated oblique angle, was placed adjacent to its target bead.

Examples of images, showing needle placement in the phantoms, are provided in Figure 4.

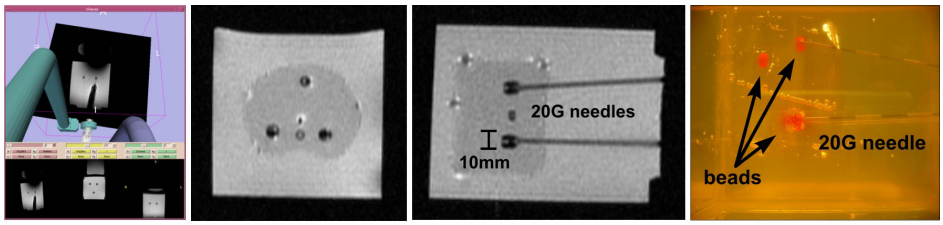

Figure 4. (a) Real-time image visualization in the Slicer interface during needle insertion; (b,c) MRI images of needle placement in the phantom; and (d) the target phantom.

In experiments, the system consistently placed needles to within 2mm of their intended targets in a tissue phantom. Increased placement error was found for severely oblique needle trajectories, largely due to calibration errors between the optical tracker and the needle holder. This has subsequently been ameliorated through improved calibration. In general, system performance is dependent on accurate calibration between the optical tracker and the image coordinate space, as is also the case for all clinical cases undertaken in the MRT. An image-based registration and tracking approach would be preferable, and can be incorporated into our present system architecture. The advantage of such a visual servo approach is that the image and device coordinate systems are explicitly registered, as opposed to a "register and shoot" approach that is dependent on calibrated external sensors.

5. Conclusion

We have developed an integrated planning system and a robotic assistant that acts as a dynamic needle guide. This approach helps to simplify workflow by providing an interactive "point and click" trajectory planning interface and an MRI-compatible robotic mechanism for precise, yet flexible needle placement. In-scanner phantom tests have been performed in order to validate system performance and needle placement, and preparations are underway for clinical trial. The system is based on a modular and extensible architecture that will be used as a testbed for the development of novel image-based navigation and visual servo techniques in open- and closed-bore MRI scanners, in order to be extended to other applications of MRI-guided percutaneous therapy in the future.

Acknowledgements

This work was partially funded by NSF ERC 9731748, NIH 5-P01-CA067165-07 and 1-U41-RR019703. We would like to thank Dan Kacher and Janice Fairhurst for scanning assistance, and Mike McKenna for assistance with Slicer programming.

References

[1] A. V. D'Amico, C. M. Tempany, R. A. Cormack, N. Hata, M. Jinzaki, K. Tuncali, M. Weinstein, and J. P. Richie, "Transperineal magnetic resonance image guided prostate biopsy," in *Journal of Urology*, vol. 164(2), pp. 385–387, Aug. 2000.

[2] A. V. D'Amico, R. A. Cormack, and C. M. Tempany, "MRI-guided diagnosis and treatment of prostate cancer," in *New England Journal of Medicine*, vol. 344(10), pp. 776–777, Mar. 2001.

[3] K. Masamune, E. Kobayashi, Y. Masutani, M. Suzuki, T. Dohi, H. Iseki, and K. Takakura, "Development of an MRI-compatible needle insertion manipulator for stereotactic neurosurgery," in *Journal of Image Guided Surgery*, vol. 1(4), pp. 242–248, 1995.

[4] A. Felden, J. Vagner, A. Hinz, H. Fischer, S. O. Pfleiderer, J. R. Reichenbach, and W. A. Kaiser, "ROBITOM-robot for biopsy and therapy of the mamma," in *Biomedical Technology*, vol. 47, pp. 2–5, 2002.

[5] E. Hempel, H. Fischer, L. Gumb, T. Hohn, H. Krause, U. Voges, H. Breitwieser, B. Gutmann, J. Durke, M. Bock, and A. Melzer, "An MRI-compatible surgical robot for precise radiological interventions," in *Computer Aided Surgery*, pp. 180–191, Apr. 2003.

[6] K. Chinzei, N. Hata, F. A. Jolesz, and R. Kikinis, "MR compatible surgical assist robot: system integration and preliminary feasibility study," in *Medical Image Computing and Computer Assisted Intervention*, vol. 1935, pp. 921–933, Oct. 2000.

[7] S. P. DiMaio, S. Pieper, K. Chinzei, G. Fichtinger, C. Tempany, and R. Kikinis, "Robot assisted percutaneous intervention in open-MRI," in 5^{th} *Interventional MRI Symposium*, p. 155, 2004.

[8] A. Krieger, R. C. Susil, C. Menard, J. A. Coleman, G. Fichtinger, E. Atalar, and L. L. Whitcomb, "Design of a novel MRI compatible manipulator for image guided prostate interventions," in *IEEE Trans. on Biomedical Engineering*, vol. 52, pp. 306–313, Feb. 2005.

[9] G. Ganesh, R. Gassert, E. Burdet, and H. Bleule, "Dynamics and control of an MRI compatible master-slave system with hydrostatic transmission," in *International Confennee on Robotics and Automation*, pp. 1288–1294, Apr. 2004.

[10] D. Stoianovici, "Multi-imager compatible actuation principles in surgical robotics," in *International Journal of Medical Robotics and Computer Assisted Surgery*, vol. 1, pp. 86–100, 2005.

[11] N. Hata, M. Jinzaki, D. Kacher, R. Cormak, D. Gering, A. Nabavi, S. G. Silverman, A. V. D'Amico, R. Kikinis, F. A. Jolesz, and C. M. Tempany, "MRI imaging-guided prostate biopsy with surgical navigation software: device validation and feasibility," in *Radiology*, vol. 220(1), July 2001.

[12] K. Chinzei, R. Kikinis, and F. A. Jolesz, "MRI Compatibility of Mechatronic Devices: Design Criteria," in *International Conference on Medical Image Computing and Computer-Assisted Intervention (MICCAI)*.

[13] K. Chinzei, N. Hata, F. A. Jolesz, and K. Kikinis, "MRI Compatible Surgical Assist Robot: System Integration and Preliminary Feasibility Study," in *International Conference on Medical Image Computing and Computer-Assisted Intervention (MICCAI)*.

[14] K. Chinzei, N. Hata, F. Jolesz, and R. Kikinis, "Surgical Assist Robot for the Active Navigation in the Intraoperative MRI: Hardware Design Issues," in *Proceedings of the IEEE/RSJ IROS*, pp. 727–732, 2000.